INTERNATIONAL
Agrophysics
www.international-agrophysics.org

Int. Agrophys., 2026, 40, 437-447
doi: 10.31545/intagr/225059

Multispectral and image measurement for monitoring citrus growth

Takaharu Kameoka[1,2], *Shinichi Kameoka*[1,2], *Ryoei Ito*[1], *Atsushi Hashimoto*[1]*

[1]Graduate School of Bioresources, Mie University, 1577 Kurimamachiya-cho, 514-8507, Tsu, Japan
[2]General Affairs Department, ALFAE, General Incorporated Association, 7-15-8-406 Ginza, Chuo-ku, 104-0061, Tokyo, Japan

Received March 30, 2026; accepted June 25, 2026

Abstract. In fruit cultivation, simple, non-destructive, and pretreatment-free measurement techniques are essential for direct field assessments. This study aimed to develop multispectral and colour imaging methods for extremely early-maturing Satsuma mandarin (*Citrus unshiu* Marc.) and evaluate seasonal changes in fruit quality. Over two consecutive seasons (2018 and 2019), mid-infrared (MIR) and X-ray fluorescence (XRF) spectral analyses were conducted on leaves and fruit at various growth stages, alongside reference analyses of surface colour, Brix, and titratable acidity. Consistent seasonal trends were observed across both years. XRF detected significant differences in elemental content between new and old leaves, and distinct flesh colour transitions were confirmed across growth stages. Multiple regression analysis showed that juice composition could be predicted from flesh colour, yielding leave-one-cluster-out cross-validated coefficients of determination (R^2) of 0.71-0.89 (2018) and 0.75-0.96 (2019). Furthermore, total harvest sugar content per fruit was predictable from the leaf K/Ca ratio during the May fruit-set stage ($R^2 = 0.88$, cross-validated $Q^2 = 0.71$). These findings identify hue as a stable maturation indicator and demonstrate a mechanistically interpretable relationship between the leaf K/Ca ratio and harvest sugar mass, supporting classical concepts of phloem transport physiology.

Keywords: quality, infrared spectroscopy, X-ray fluorescence spectroscopy, cultivation management, Satsuma mandarin orange

1. INTRODUCTION

In fruit tree cultivation, management practices have traditionally relied on growers' experience and intuition. However, such qualitative approaches are increasingly insufficient under conditions of labour shortage and climate variability, necessitating the transition to quantitative and objective field-based indicators (Kameoka *et al.*, 2017; Muramatsu *et al.*, 2020). Evergreen fruit trees such as Satsuma mandarin present additional complexity because the physiological conditions of leaves and fruit change continuously and interactively over multiple years (Spiegel-Roy and Goldschmidt, 1996). Traditional destructive analyses are time-consuming and unsuitable for real-time orchard management; thus, rapid non-destructive measurement methods without pretreatment are highly desirable.

Optical sensing techniques, including mid-infrared (MIR) spectroscopy, colour image analysis, and X-ray fluorescence spectroscopy (XRF), have shown great promise in fruit quality evaluation. MIR spectroscopy provides molecular-level information, specifically within the 1 300-1 000 cm^{-1} fingerprint region, where distinct absorption bands allow the simultaneous discrimination of organic acids (citric and malic) and sugars (glucose, sucrose, and fructose) (Bureau *et al.*, 2009; Kameoka *et al.*, 1998;

*Corresponding author e-mail: hasimoto@bio.mie-u.ac.jp

Zaresani *et al.*, 2024). Qualitative and quantitative MIR spectroscopic methods for these components in fruit juices have been developed previously (Kameoka *et al.*, 1998; Kanou *et al.*, 2017; Nakanishi *et al.*, 2003; Yajima *et al.*, 2024). XRF enables elemental analysis of plant tissues, tracking the seasonal accumulation of inorganic elements such as phosphorus (P), potassium (K), and calcium (Ca) (McLaren *et al.*, 2012; Mizuno *et al.*, 2024; Reidinger *et al.*, 2012). Colour image analysis offers practical indicators of maturation and quality (Motonaga *et al.*, 2004; Yamamoto *et al.*, 2014); for instance, the steady decrease in hue (H) and the increase in saturation (S) provide a quantitative description of the transition from early developmental stages to harvest readiness (Khojastehnazhand *et al.*, 2009; Mendoza *et al.*, 2006; Pathare *et al.*, 2013). By integrating these molecular, elemental, and colorimetric parameters, a high-fidelity analysis of both leaves and fruit can be achieved.

Most previous studies have focused on a single sensing modality or analysed leaves and fruit in isolation. As a result, the physiological linkage between leaf nutrient status and compositional changes in fruit has not been sufficiently quantified. Although the weight percentage of minerals in developing fruit may decrease through dilution, the total amount of these elements continues to rise. Previous observations indicate that new and old leaves exhibit distinct seasonal accumulation patterns of Ca and K, which directly influence the final quality of fruit. There remains a lack of integrated studies that simultaneously and longitudinally analyse leaves and fruit using multiple optical sensing techniques, although a small number of reports have combined molecular, elemental, and colorimetric information to estimate fruit quality in a physiologically interpretable manner (Kameoka and Hashimoto, 2015; Muramatsu *et al*., 2020).

The present research focused on two primary objectives to bridge the gap between sensing technology and physiological insight. First, the development of field-ready protocols for non-destructive measurements was sought, ensuring the accuracy of MIR for juice components and XRF for fresh-sample analysis. Second, a comprehensive quality evaluation system based on a two-year longitudinal study was to be established. The extremely early-maturing Satsuma mandarin was selected for the present investigation because its compressed developmental schedule, with fruit-set in May and harvest in October, renders the temporal coupling between early-season leaf physiology and late-season fruit composition empirically tractable within a single growing season.

2. MATERIALS AND METHODS

2.1. Sample plants

The experiment was conducted on extremely early-maturing Satsuma mandarin trees (*Citrus unshiu* Marc.) grown in an experimental orchard at the Kanayama Pilot Farm in Kumano, Mie Prefecture, Japan, from May 2018 to October 2019. Three trees were selected, and each tree was divided into three clusters based on main branches, yielding a total of nine clusters. For each sampling event, three leaves per cluster (27 leaves in total) and one fruit per cluster (nine fruits in total) were collected, as shown in Fig. 1. In 2018, only new-flush leaves were sampled; in 2019, both new-flush and old-flush (previous-season) leaves were sampled from identical clusters to facilitate comparison of the two leaf populations. New-flush leaves were distinguished from old-flush leaves on the basis of leaf colour intensity, leaf-blade thickness, and position on the shoot.

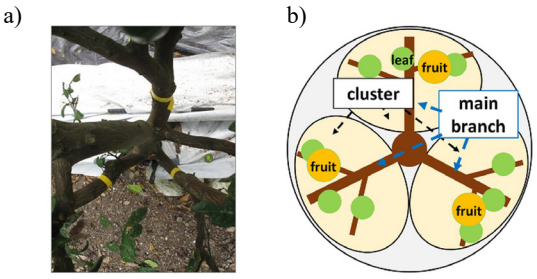

Fig. 1. Experimental sampling unit: a) an example of RGB photograph of a representative experimental tree, b) schematic representation of the sampling unit.

Sampling was conducted once per month. Leaves were collected from the fruiting season to the harvest season, and fruit were sampled from the cell-enlargement stage through harvest. Measurements were performed over two consecutive years, facilitating the evaluation of temporal trends and year-to-year reproducibility.

2.2. MIR spectroscopic measurements

Fruit juice was obtained by squeezing fresh fruit, followed by centrifugation at 6200 rpm for 20 min. No chemical pretreatment was applied to preserve the simplicity of the method. A Fourier-transform infrared spectrometer (FTIR; Spectrum Two, PerkinElmer Inc., Waltham, MA, USA) equipped with a single-reflection attenuated total reflection (ATR) accessory was used to collect the MIR absorption spectra of the juice. Eight scans of symmetrical interferograms at a 2 cm^{-1} resolution were co-added for each spectrum in the range of 4 000-400 cm^{-1}.

Characteristic absorption bands for saccharides (1 000-1 200 cm^{-1}) and organic acids (1 200-1 300 cm^{-1}) were used for component analysis. The characteristic absorption coefficients of glucose, sucrose, fructose, citric acid, and malic acid in an aqueous solution were determined from pure-component reference spectra of the corresponding guaranteed-reagent-grade standards (Wako Pure Chemical Industries, Ltd., Osaka, Japan; now FUJIFILM Wako Pure Chemical Corporation) over the concentration ranges relevant to fruit juice (1-10 wt% for sugars and 0.1-4 wt% for acids), following the procedure of Kameoka *et al.* (1998)

and Kanou *et al.* (2017). Classical least-squares (CLS) regression was applied to the pre-processed spectra to estimate sugar and acid contents using the following equations:

$$A = CK, \quad (1)$$

$$C = AK^T (KK^T)^{-1}, \quad (2)$$

where: A, C, and K are the absorbance matrix, the solute concentration matrix, and the absorptivity matrix, respectively. Wavenumber selection and model evaluation were based on the coefficient of determination (R^2), with all final calibration models yielding $R^2 > 0.97$. The accuracy of this MIR/CLS approach was established in earlier work, in which calibration of the individual sugars against pure-component standards yielded R^2 values of 0.997-0.998 and an average standard error of calibration of 0.34 wt% (Kameoka *et al.*, 1998).

2.3. X-ray fluorescence measurements

Elemental analysis of leaves, pericarps, and fruit juice was performed using a portable X-ray fluorescence analyser (Innov-X DELTA Premium Handheld XRF; Olympus Corporation, Tokyo, Japan) mounted on a dedicated measurement station developed in previous studies (Kameoka *et al.*, 2017; Muramatsu *et al.*, 2020). Measurements focused on K, Ca, and P. The instrument operated in two energy ranges – Beam 1 (0-40 keV) for heavier elements and Beam 2 (0-10 keV) for lighter elements – with rhodium-based intensity correction applied to both. Elemental contents were calculated using the fundamental-parameter (FP) method, which accounts for X-ray energy, fluorescence yield, and matrix effects.

Instrument calibration was verified against the certified reference material NMIJ CRM 7505-a (No. 122, tea-leaf powder), prepared as a leaf model by packing the powder into a 14 mm-diameter aperture machined into a 3 mm plastic board (PLA-BOARD, Tamiya Inc., Shizuoka, Japan) sealed with X-ray-transparent film (Prolene Thin-Film, Chemplex Industries Inc., Palm City, FL, USA), and packed at a density of 0.108 g cm^{-3}. For the measurement of plant tissue with a low effective atomic number, the standard stainless-steel docking-station coin was replaced by a 99.6% titanium coin to minimise spurious contributions from the calibration substrate, as titanium is absent from healthy citrus leaf tissue and is detectable in both beam ranges.

For accurate XRF quantification of fresh plant material, the sample thickness must exceed the half-attenuation layer $t_{1/2}$ at the relevant photon energy, defined as the sample thickness at which the transmitted X-ray intensity is reduced to one-half of the incident intensity (Nakai *et al.*, 2016). The half-attenuation layer was computed from the Beer-Lambert relation as:

$$t_{1/2} = \frac{ln2}{\mu_M \rho}, \quad (3)$$

where: μ_M (cm^2 g^{-1}) is the mass attenuation coefficient of the sample and ρ (g cm^{-3}) is the sample density. The mass attenuation coefficient of the multi-component sample was computed as the mass-weighted sum of the coefficients of the constituent components:

$$\mu_M = \Sigma_i (w_i \mu_i), \quad (4)$$

where: w_i is the mass fraction of component i in the sample and μ_i (cm^2 g^{-1}) is the mass attenuation coefficient of component i at the relevant photon energy. For Satsuma mandarin leaves, the constituent components were taken as water, cellulose, and the principal mineral elements (N, P, K, Ca, Mg), with the mass fractions of the mineral elements based on standard horticultural reference values for Satsuma mandarin leaves. The leaf was assumed to consist of water at a mass fraction of 0.613 (the measured mean gravimetric moisture content), with the remaining solid fraction approximated as cellulose plus the measured mineral fractions. The mean leaf density was determined experimentally as 1.08 g cm^{-3}. Application of Eqs (3) and (4) to the leaf composition yielded a half-attenuation layer of 0.242-0.322 mm at a photon energy of 4 keV and of 0.387-0.516 mm at 5 keV; the measured mean leaf thickness of 0.292 mm therefore satisfies the threshold for elements with characteristic X-ray energies below approximately 4 keV (*i.e.*, for elements up to and including Ca, atomic umber $\leq$ 20). The XRF-derived elemental values are expressed as mass percent [wt%] on a dry-weight basis throughout the present manuscript, computed from the as-measured fresh-weight values via the moisture-content correction described above.

2.4. Colour image measurement

Colour images of fruit and flesh cross-sections were acquired using a digital camera (D300, Nikon Corporation, Tokyo, Japan) mounted at the centre of a white cylindrical diffuse reflector. Illumination was provided by two fluorescent lamps (VITA-LITE, USA L.S. Co., Ltd, USA) at a correlated colour temperature of 5 500 K, in accordance with CIE (Commission Internationale de l'Eclairage) recommendations for colour measurement. Samples were positioned directly beneath the camera and within the cylindrical reflector so as to lie close to the centre of the image field. White balance was verified before each session using a reference white panel placed at the sample position. Images were recorded in RAW format. Sample regions were extracted using Photoshop CS4 (Adobe Inc., San Jose, CA, USA) and saved as 8-bit TIFF files. The RGB values in the RGB colour space were obtained for each pixel of the extracted image, and the average values were calculated for colour-parameter evaluation.

OpenCV, an open-source computer-vision library, was used for the analysis of images acquired by the colour image measurement system. Images of mandarin fruit

cross-sections were extracted by generating mask images based on saturation values. The flesh region was specifically isolated using hue, saturation, and value (*HSV*) values to obtain its colour information. The acquired *RGB* colour data were then converted into the *HSV* and *L*a*b** colour spaces for further analysis. The output ranges were 0–255 for *RGB*, 0-180 for *H*, and 0-255 for both *S* and *V*. For the *L*a*b** colour system, *L** ranged from 0 to 100, while *a** and *b** ranged from -127 to 127. The representative value for the flesh was defined as the mean across the masked region, rounded to one decimal place.

2.5. Reference analyses

2.5.1. Measurement of Brix

A pocket refractometer (PAL-1, Atago Co., Ltd., Tokyo) was used to measure the Brix value. For each sample, 0.3 mL of fruit juice was collected and measured. Measurements were performed in triplicate for each sample, and the average value was used as the representative value. The Brix value represents the total soluble solids (TSS) of the juice, which in citrus comprises sugars together with organic acids, amino acids, and other minor solutes whose relative proportions change during fruit development (Ting, 1969; Ting and Rouseff, 1986). Accordingly, Brix was used here only as a conventional reference index of TSS and was not equated with the total sugar content.

2.5.2. Measurement of titratable acidity

Titratable acidity was determined by titrating 10 mL of clarified juice with 0.1 mol L^{-1} NaOH to a phenolphthalein endpoint (pH 8.1) and was expressed as g citric acid equivalent per 100 mL juice. Total sugar content per fruit was obtained from the MIR-derived total sugar concentration (the sum of glucose, sucrose, and fructose quantified by the CLS model) multiplied by the total juice mass extracted from each fruit; it was therefore determined independently of the refractometric Brix measurement.

2.5.3. Inductively coupled plasma optical emission spectrometry (ICP-OES) measurement

A subset of leaf samples was analysed by inductively coupled plasma optical emission spectrometry (ICP-OES) following acid digestion. An ICP optical emission spectrometer (5110 ICP-OES, Agilent Technologies, Ltd.) was employed as a conventional method for elemental analysis of plant samples. The leaves were placed in a dryer set at 373 K and dried for a full day. The dried leaves were ground into a powder using a mortar and pestle, and 0.25 g of the resulting powder was transferred into a 30 mL Kjeldahl flask. Subsequently, 2 mL of concentrated sulphuric acid and 1 mL of hydrogen peroxide solution were added. The flask was then placed on a heater preheated to 473 K for digestion.

Since the boiling point of hydrogen peroxide is approximately 426 K, the flask was removed from the heater once the hydrogen peroxide had completely boiled off, foaming had subsided, and the solution turned brown. After cooling, an additional 1 mL of hydrogen peroxide was added, and heating was resumed. This digestion process was repeated until the foaming ceased and the solution became colourless and transparent. After digestion, a small amount of pure water was added to dilute the solution, followed by filtration using filter paper. The filtrate was then diluted to a final volume of 50 mL with pure water in a volumetric flask to prepare the analytical sample.

2.6. Statistical analysis

All statistical analyses were performed in Python 3 (SciPy and statsmodels), with statistical significance set at $p < 0.05$. Differences in leaf Ca and K content between new and old leaves were evaluated by Welch's t-test (N = 3 trees per leaf type). The colour-based multiple-regression models for juice composition were validated by leave-one-cluster-out cross-validation, with the mean coefficient of determination (R^2) and root-mean-square error reported across the three folds. The relationship between the leaf K/Ca ratio at fruit set and the total sugar content per fruit at harvest (N = 6) was assessed by an F-test of the regression, Spearman's rank correlation, leave-one-out cross-validation (Q^2 and RMSECV), and a Fisher z-transformed 95% confidence interval.

3. RESULTS

3.1. MIR spectroscopic analysis of fruit juice

Figure 2 shows the MIR absorbance spectra of pure-component reference standards (panel a) and the corresponding measured-versus-estimated scatter plot for the developed CLS model applied to fruit-juice samples (panel b). The

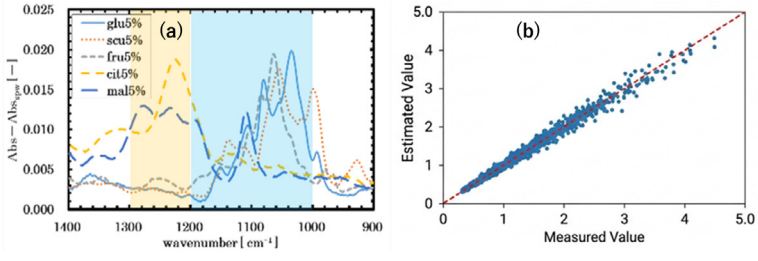

Fig. 2. MIR absorbance spectra of major components in fruit juice and content determination: a) reference spectra of sugars and organic acids, b) comparison between measured and estimated values using the developed MIR spectroscopic model.

data points are tightly clustered along the 1:1 identity line across the entire range from 0 to 5 wt%, demonstrating that the model accurately estimates the target internal quality parameters with minimal bias.

3.2. Seasonal changes in juice composition

Figure 3 illustrates the changes in the chemical composition of mandarin fruit juice over the two-year cultivation period. Panel (a) shows the relationship between total sugar and total acid concentrations, while panel (b) details the trends of the individual sugar components: sucrose, glucose, and fructose. Panel (a) reveals a clear inverse correlation between sugar and acid levels. Throughout the two-year period, the total sugar concentration steadily increased from approximately 2.8 wt% at the early developmental stage (DAFB 55 d) to 9.7 wt% at harvest (DAFB 175 d). Conversely, the total acid concentration showed a consistent decline, falling from approximately 3.4 wt% at DAFB 55 d to 1.4 wt% at DAFB 175 d.

In Fig. 3b, the concentrations of specific sugars are analysed. Sucrose exhibited a significant and continuous rise, increasing from approximately 1.8 to 4.9 wt% by the end of the sampling period. In turn, glucose and fructose followed similar trajectories, rising from approximately 0.5 wt% to a plateau of approximately 2.0-2.5 wt% by DAFB 150 d.

3.3. Elemental changes in leaves and pericarp during fruit growth

Figure 4 shows the time courses of elemental content in leaves over the two years. Distinct temporal patterns were observed for each element. New leaves and old leaves exhibited significantly different elemental contents. At the fruit-set stage, this difference was statistically significant for both Ca and K (Welch's t-test, $p < 0.001$ for each; $N = 3$ trees per leaf type), with new leaves also showing a markedly higher leaf K/Ca ratio than old leaves ($p < 0.05$). Despite the year-to-year variation in absolute values, the overall trends were reproducible across both years. The Ca content in new leaves exhibited a steady, monotonic increase from approximately 0.9 wt% in May (DAFB 20 d) to approximately 2.3 wt% by October (DAFB 152 d), reflecting the cumulative xylem-mediated deposition of Ca within the cell-wall pectin matrix. The Ca content in old leaves remained consistently high at approximately 3.0-3.5 wt% throughout the growing season, indicating that calcium accumulated in the previous growing season is

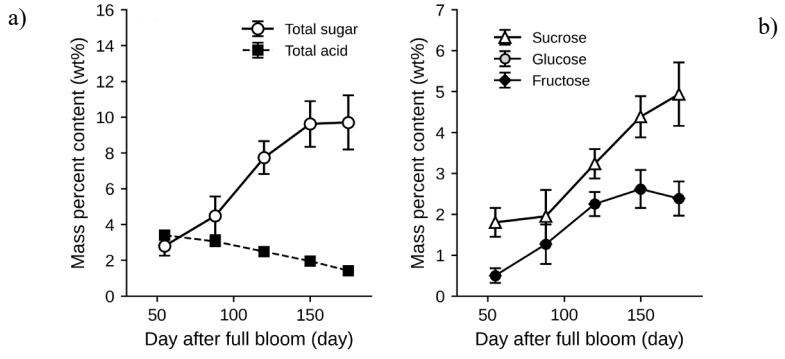

Fig. 3. Seasonal changes in sugar and organic acid concentrations over two years: a) total sugars and total acids; b) sucrose, glucose, and fructose.

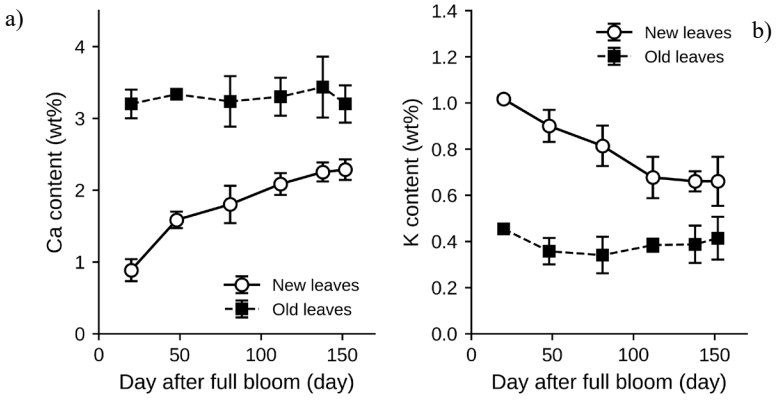

Fig. 4. Seasonal changes in: a) calcium and b) potassium contents in new and old leaves of Satsuma mandarin (*C. unshiu* Marc.). Data are plotted against days after full bloom and span the 2018 and 2019 growing seasons, new leaves were sampled in both years, whereas old leaves were sampled in 2019 only. Error bars represent ± 1 SD of the replicate leaf measurements at each sampling time.

retained essentially unchanged. Old leaves consistently maintained higher Ca content than new leaves throughout the growing season. The K content in new leaves showed a steady decline from approximately 1.0 wt% in May (DAFB 20 d) to approximately 0.65 wt% by October (DAFB 152 d), reflecting the progressive translocation of K from leaf tissue to developing fruit. The K content in old leaves remained low and stable at approximately 0.35-0.45 wt% throughout the growing season. New leaves consistently exhibited higher K content than old leaves, consistent with the role of newly expanded foliage as the principal source organ for phloem-mediated potassium transport.

These distinct accumulation patterns reflect the physiological nutrient requirements of the tree during fruit development. The differential elemental contents between new and old leaves provide critical data for calculating the K/Ca ratio, which serves as a physiological indicator for predicting fruit quality at harvest.

Figure 5 shows the time courses of elemental content and total amount in pericarps after full bloom. The elemental contents in the pericarp showed a non-monotonic accumulation pattern: Ca and K contents increased rapidly from approximately 0.07 and 0.20 wt% at DAFB 55 d to a maximum of approximately 0.50 and 0.43 wt% at DAFB 90-120 d, and then declined moderately or stabilised throughout harvest. The P content followed a similar pattern at a lower magnitude, increasing from approximately 0.03 wt% to a plateau of approximately 0.08 wt%. In contrast, the absolute amounts of K, Ca, and P per fruit increased monotonically during development. Among the three elements, Ca attained the highest peak content, followed by K, with P remaining at a lower magnitude throughout the growing period.

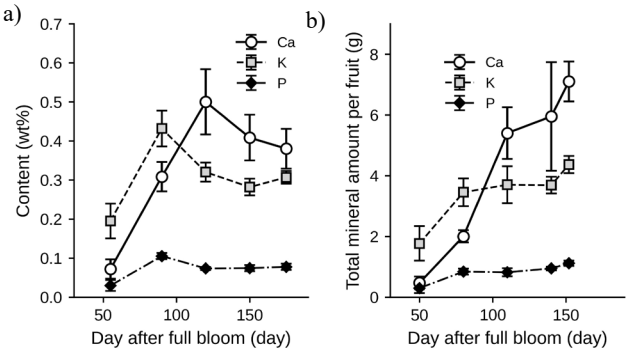

Fig. 5. Changes in mineral: a) contents and b) total amounts in pericarps after full bloom. Pericarps were sampled across the 2018 and 2019 growing seasons: a) shows the elemental content (wt%) and b) shows the corresponding total amount per fruit (g), both plotted against days after full bloom. Error bars represent ± 1 SD of the replicate fruit measurements at each sampling time.

The total amounts of Ca, K, and P per fruit increased monotonically with the number of days from full bloom, reflecting a steady and continuous uptake of these nutrients from the tree to the fruit during the developmental stages. Ca exhibited the largest absolute increase, from approximately 0.5 g per fruit at DAFB 50 d to 7.1 g per fruit at DAFB 152 d, consistent with the role of Ca as a cell-wall structural component progressively incorporated into the pectin matrix of the expanding pericarp. K and P showed parallel but smaller absolute accumulations, consistent with their respective roles as osmotic and energetic constituents.

3.4. Changes in flesh colour during maturation

In Figure 6a, the photographs illustrate the clear transition of fruit flesh and rind colour from pale green or yellow (June) to deep orange (October), marking the progress of the maturation stage. The *H* value steadily decreased from approximately 29.3 (DAFB 50 d) to 14.0 (DAFB 170 d) as the number of days after full bloom progressed. The corresponding visual change from greenish to reddish-orange is shown in Fig. 6b. The *S* value in Fig. 6c showed a significant upward trend, indicating that the fruit colour became increasingly vivid and intense as harvest time approached. Error bars (± 1 SD across the six tree-year measurement curves; three trees × two years) are shown in Fig. 6b and c.

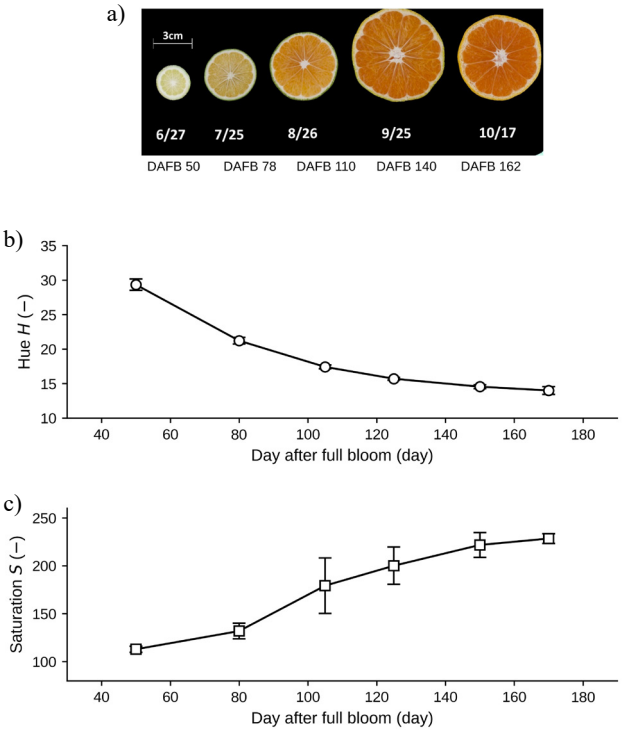

Fig. 6. Quantitative analysis of colour changes in fruit cross-sections from June to October: a) visual appearances, b) hue change, c) saturation change. Error bars in panels b) and c) represent ± 1 SD across the six tree-year measurement curves.

3.5. Estimation of fruit quality from optical information

3.5.1. Estimation based on flesh colour

Based on the results shown in Fig. 6, the relationship between the internal quality of the fruit and the colour information was studied. Figure 7 highlights the robust performance of a multivariate model in which total sugar content is expressed as a function of *H* and *S* values. The data points move along the regression line from the bottom-left (July) to the top-right (October), reflecting the natural physiological increase in sugar levels as the fruit matures. Despite the significant changes in fruit appearance over the four-month period, the predicted sugar content aligns closely with the measured values across the entire maturation range (approximately 3 to 15 wt%). These results suggest that external colorimetric data can serve as a reliable proxy for internal carbohydrate accumulation, enabling rapid and non-destructive quality monitoring in the field.

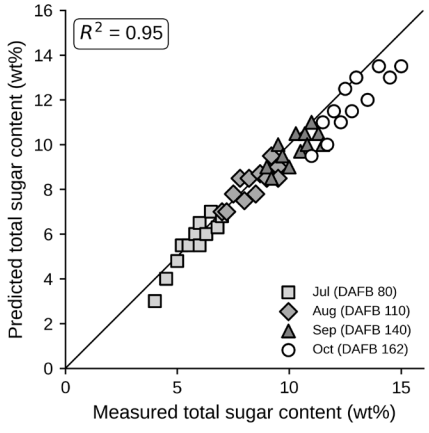

Fig. 7. Prediction of total sugar content based on fruit colour dynamics. The displayed $R^2 = 0.95$ is the pooled fit across both growing seasons and the full developmental range; by leave-one-cluster-out cross-validation, the per-year predictive accuracy was $R^2 = 0.72$ (RMSE = 0.92 wt%) in 2018 and 0.90 (RMSE = 0.99 wt%) in 2019.

For the systematic statistical validation of these multiple-regression models, leave-one-cluster-out cross-validation was performed (k = 3 folds, corresponding to the three orchard clusters established in the sampling design). In each iteration, two clusters were used to estimate the partial regression coefficients while the remaining cluster was used for validation, and this procedure was repeated three times with the validation cluster rotated. The mean coefficient of determination R^2 across the three folds is reported below. The 2018 calibration yielded cross-validated R^2 values in the range of 0.71-0.89 across nine response variables, with the strongest performance obtained for the sugar to acid ratio ($R^2 = 0.89$), citric acid content ($R^2 = 0.86$), and titratable acidity ($R^2 = 0.86$); the weakest performance was observed for sucrose content ($R^2 = 0.71$). The 2019 calibration yielded cross-validated R^2 values in the range of 0.75-0.96 across fourteen response variables, with the strongest performance obtained for titratable acidity ($R^2 = 0.96$), total acid content ($R^2 = 0.96$), and citric acid content ($R^2 = 0.95$); the weakest performance was found for malic acid content ($R^2 = 0.75$). All response variables in both years exceeded the threshold of $R^2 \geq 0.70$, indicating that flesh colour information provides a robust predictive basis for juice composition within a given growing season. For total sugar specifically, leave-one-cluster-out cross-validation gave $R^2 = 0.72$ (RMSE = 0.92 wt%) in 2018 and 0.90 (RMSE = 0.99 wt%) in 2019; the close agreement between these cross-validated values and the corresponding calibration-fit adjusted R^2 (0.75 and 0.91) indicates negligible optimism and no appreciable overfitting. In the full-season regression, hue was the dominant, statistically significant predictor of total sugar in 2019 ($p < 0.001$), whereas neither colour coefficient reached significance in 2018 ($p > 0.2$), consistent with the year-specific behaviour of sugar prediction.

To assess the temporal stability of the calibration models across growing seasons, cross-year prediction was independently performed: the regression model calibrated on the 2018 data was applied to the 2019 dataset, and the model calibrated on the 2019 data was applied to the 2018 dataset. The cross-year prediction yielded markedly different performance between acid-related and sugar-related response variables. Acid-related variables exhibited robust cross-year transfer, with prediction $R^2 = 0.83$ (total acid), 0.82 (citric acid), and 0.78 (titratable acidity) when the 2018 model was applied to the 2019 data, and $R^2 = 0.88$ (total acid), 0.90 (malic acid), and 0.88 (Brix − titratable acidity) when the 2019 model was applied to the 2018 data. In contrast, sugar-related variables exhibited substantially degraded cross-year transfer, with several models yielding negative R^2 values when applied across years, indicating that the partial regression coefficients for sugars are year-specific. The biological basis for this contrast between acid and sugar predictability is considered in the Discussion.

3.5.2. Estimation based on leaf elemental information

Figure 8 shows the relationship between the leaf K/Ca ratio at the fruit-set stage in May and the total sugar content per fruit at harvest in October for six tree-year observations (three trees over two consecutive growing seasons). A significant positive linear regression was obtained, with a coefficient of determination of $R^2 = 0.88$. The corresponding regression equation was $y = 9.86\ x - 1.46$, where y denotes the total sugar content per fruit (g) and x denotes the leaf K/Ca ratio (-). No equivalent relationship was detected when K or Ca was considered as independent variables; the predictive association became apparent only after the two elements were combined into their ratio and the fruit-side

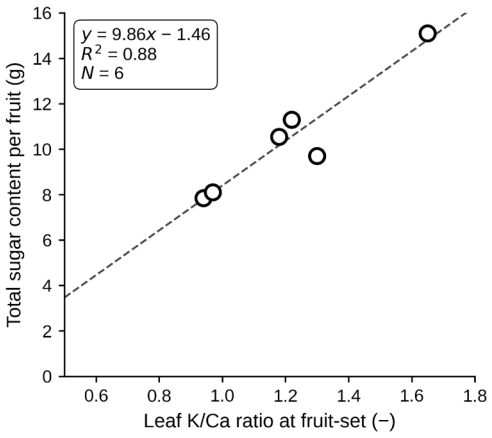

Fig. 8. Relationship between the leaf K/Ca ratio at the fruit set stage in May and the total sugar content per fruit at harvest in October for six tree year observations (2018 trees 1-3, 2019 trees 1-3). Linear regression: y = 9.86 x − 1.46, R^2 = 0.88, N = 6. Dashed line shows the fitted regression.

response variable was expressed on a per-fruit total-mass basis rather than as a concentration in juice. This observation indicates that the K/Ca ratio operates as a compound state variable integrating information not retrievable from the individual elemental measurements.

4. DISCUSSION

4.1. Mechanistic interpretation of the leaf K/Ca ratio as a systemic state variable

The mechanistic basis of the predictive relationship shown in Fig. 8 is interpretable through the contrasting transport behaviour of K^+ and Ca^{2+} in the long-distance vascular system of higher plants. K^+ exhibits high phloem mobility, whereas Ca^{2+} is essentially phloem-immobile and is delivered to the leaf almost exclusively through the transpiration-driven xylem stream, after which it is fixed within the cell-wall pectin matrix. Zimmermann and Milburn (1975) proposed that long-distance carbohydrate translocation through the phloem is accompanied by a solution of high K/Ca ratio, with K^+ functioning as the principal counter ion that maintains electroneutrality during phloem loading and unloading and sustains the osmotic gradient driving mass flow. Under this view, the K^+ economy of source leaves is mechanistically coupled to the leaf's instantaneous phloem-loading capacity, while the leaf Ca^{2+} content reflects the time integral of xylem-mediated delivery up to that point.

When the antagonistic uptake of these two cations at the root surface (Najafi-Ghiri *et al.*, 2022) is additionally taken into account, the leaf K/Ca ratio is shown to constitute a systemic state variable that integrates three sequential physicochemical processes: differential absorption at the rhizosphere, differential transport through the xylem and phloem, and differential accumulation within the leaf tissue. Under this interpretation, the leaf K/Ca ratio operates as a dimensionless quantity that normalises the currently active phloem-loading capacity by the cumulatively established xylem-mediated mineral accumulation. The predictive relationship between this ratio at fruit-set and harvest sugar content is then interpretable as a causal chain extending over the developmental season: the phloem-loading capacity established at fruit-set determines the throughput of photoassimilate transport during the subsequent fruit-filling period, which is registered as the final sugar mass of the harvested fruit. The differences between new and old leaves observed in Fig. 4 reflect the distinct functional roles of these two leaf populations in nutrient storage and active translocation.

4.2. Comparison with previously published work

The present finding is consistent with several independent lines of evidence in the published literature. The asymmetry in transport characteristics between these two ions – K^+ being highly phloem-mobile and Ca^{2+} being essentially phloem-immobile – has been established as a fundamental tenet of plant physiology (Albrigo, 2019; Marschner, 2011; Taiz and Zeiger, 2017). Through tissue-level mineral analysis of navel orange (*Citrus sinensis*), Storey and Treeby (2000) reported that K and Ca exhibit contrasting accumulation patterns between flesh and peel during fruit development, with the flesh maintaining a higher K/Ca ratio than the peel throughout the season – a pattern directly explicable by the differential transport mechanism described above.

Dilmaghani *et al.* (2005) reported a correlation between the leaf K/Ca ratio and fruit firmness in apple, a quality parameter likewise governed in part by phloem-delivered carbohydrate metabolism and cell-wall calcium incorporation. The convergence of the present finding with the apple result across phylogenetically distant fruit species and across different quality attributes supports the proposition that the leaf K/Ca ratio operates as a generalisable indicator of phloem transport capacity rather than as a species or quality parameter specific correlate.

Further independent support derives from controlled nutrient-solution experiments in strawberry, in which solutions of elevated K/Ca ratio produced fruit of higher quality across multiple cultivars (Lieten, 2006; Khalil *et al.*, 2020). These experiments operated at the level of the nutrient solution rather than the leaf tissue, providing independent experimental confirmation that the K/Ca stoichiometry of the plant's mineral economy is causally – rather than merely correlationally – linked to fruit composition. The present observational study extends this body of evidence by demonstrating that the corresponding relationship can be detected at the tissue level (leaf K/Ca) without imposed nutrient-solution manipulation and at an early developmental stage (May) that precedes the harvest stage (October) by approximately five months. To the knowledge of the present authors, the predictive relationship between an early-

season leaf K/Ca measurement and end-of-season fruit composition in Satsuma mandarin has not been previously reported.

The pericarp mineral dynamics (Fig. 5) are consistent with this transport asymmetry. The non-monotonic pattern of mineral concentration – an early active-uptake phase followed by a dilution-dominated phase as fruit biomass expands-together with the monotonic increase in the total mineral amount per fruit, parallels the seasonal nutrient redistribution reported for navel orange (Storey and Treeby, 2000) and reflects the progressive incorporation of xylem-delivered Ca into the expanding cell-wall matrix alongside continued phloem-mediated K and P influx.

4.3. Statistical robustness and limitations of the K/Ca-sugar relationship

The relationship shown in Fig. 8 was established from six tree-year observations (three trees monitored over two consecutive growing seasons). Although this sample size is consistent with the temporal and spatial scale of a single-orchard longitudinal field investigation, it is too small to permit conventional k-fold cross-validation. Three complementary tests, each appropriate for small samples, were therefore applied to assess statistical robustness (Fig. 9).

First, an F-test of the regression yielded $F(1, 4) = 27.6$, corresponding to $p = 0.006$, indicating that the observed association is statistically significant at the $\alpha = 0.01$ threshold. Second, the Spearman rank correlation coefficient was computed as an independent and distribution-free test of monotonic association and was found to be $\rho = 0.83$ ($p = 0.042$), confirming that the rank ordering of trees by leaf K/Ca at fruit-set is essentially preserved in their rank ordering by harvest sugar content. Third, leave-one-out cross-validation (LOOCV), the standard internal validation procedure for samples of $N \leq 10$, was implemented. The cross-validated predictive coefficient of determination was $Q^2 = 0.71$, with a root-mean-squared error of cross-validation (RMSECV) of 1.30 g sugar per fruit. The modest difference between R^2 (0.88) and Q^2 (0.71) indicates an acceptable degree of optimism in the calibration model and confirms that no single observation exerts a destabilising influence on the regression result. The Fisher z-transformation yielded a 95% confidence interval for the Pearson correlation of (0.51, 0.99), a wide interval reflecting the limited sample size but one that excludes zero with a substantial margin.

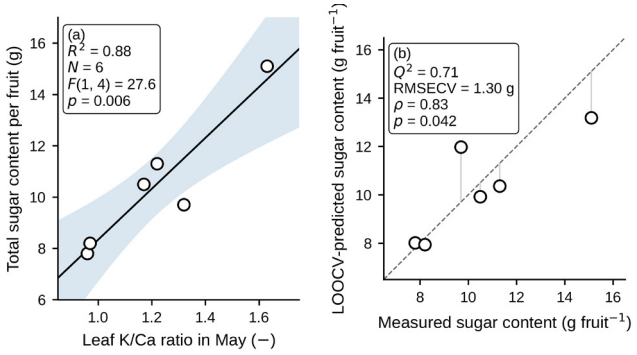

Fig. 9. Statistical validation of the relationship between the leaf K/Ca ratio at the fruit-set stage (May) and the total sugar content per fruit at harvest (October): a) linear regression with 95% confidence band, b) leave-one-out cross-validation observed versus predicted plot.

It must nevertheless be emphasised that the present findings derive from a single experimental orchard located at the Kanayama Pilot Farm in Kumano, Mie Prefecture, Japan; from a single cultivar (extremely early-maturing Satsuma mandarin, *Citrus unshiu* Marc.); and from a two-year observation window. Generalisation of the quantitative regression parameters to other cultivars, orchard environments, climatic regions, and management practices requires confirmation through independent multi-site, multi-cultivar investigations. The principal scientific contribution of the present study lies not in the establishment of a finalised predictive model, but in the empirical demonstration that the leaf K/Ca ratio operates as a candidate state variable carrying physiologically interpretable predictive information about end of season fruit composition.

4.4. Interpretation of the spectroscopic and colorimetric results

The MIR/CLS model quantified the principal sugars and organic acids of the juice directly from the absorbance spectrum without chemical pre-treatment, in agreement with earlier FTIR/ATR studies of fruit juices (Bureau *et al.*, 2009; Kanou *et al.*, 2017). The tight clustering of the measured and estimated values along the 1:1 line (Fig. 2b) indicates that the fingerprint region carries sufficient information to resolve the individual solutes, supporting MIR spectroscopy as a rapid, reagent-free alternative to chromatographic assays for in-field composition monitoring.

The colorimetric results allow a clear biological interpretation. The monotonic decline in hue with maturation (Fig. 6) reflects the degradation of chlorophyll and the accumulation of carotenoids that accompanies citrus ripening (Taiz and Zeiger, 2017), so that hue functions as an integrative optical reporter of pigment transition rather than of any single solute, and the colorimetric parameters can therefore serve as practical indicators of the ripening stage. This pigment basis also explains the contrasting cross-year behaviour of the colour-based models: acid-related variables, whose seasonal decline is coupled to the same maturation programme, transferred robustly across growing seasons, whereas sugar accumulation-governed by year-specific source-sink and environmental factors that do not directly modulate flesh colour-required annual re-calibration. Hue is therefore biologically meaningful as a maturity and acidity proxy, while colorimetric data provide only an indirect, year-dependent estimate of sugar content.

5. CONCLUSIONS

A robust non-destructive framework for evaluating fruit and leaf quality using MIR spectroscopy, XRF spectroscopy, and colour image analysis was established. By identifying specific molecular fingerprints in the 1 300-1 000 cm^{-1} range and monitoring seasonal mineral dynamics, the present study demonstrated that these techniques can reliably replace traditional destructive analyses. Although fruit mineral contents decreased through dilution, the total nutrient accumulation per fruit remained linear over time, with new leaves consistently maintaining higher Ca and K contents than old leaves throughout the growing season.

Furthermore, image-based analysis identified the hue value as a stable indicator of developmental timing and sugar accumulation, remaining unaffected by transient environmental fluctuations. Multiple-regression models for juice composition based on flesh colour information were validated by leave-one-cluster-out cross-validation, yielding coefficients of determination in the ranges of 0.71-0.89 (2018) and 0.75-0.96 (2019) across the measured response variables; cross-year prediction further demonstrated that acid-related variables exhibit robust temporal stability across growing seasons, whereas sugar-related variables reuire annual model re-calibration. Crucially, the strong linear correlation between the leaf K/Ca ratio at the fruit-set stage and the total sugar content per fruit at harvest, with a coefficient of determination of 0.88 and a cross-validated predictive coefficient of determination of 0.71, highlights the foliage's role in determining carbohydrate sink strength. The mechanistic interpretation of the K/Ca ratio as a systemic state variable integrating phloem and xylem transport processes provides a physiologically grounded basis for non-destructive monitoring. By synthesising molecular, elemental, and colorimetric data, this research provides an interpretable system for precision orchard management and optimal harvest timing. Future research will extend the present framework to additional cultivars, multi-site validation, and integration with robotic platforms for automated maturity assessment in the field.

Acknowledgements. The authors gratefully acknowledge the Kanayama Pilot Farm in Kumano, Mie Prefecture, Japan, for providing access to the experimental orchard and for ongoing cooperation throughout the two-year sampling period. The original elemental and quality measurements that constitute the empirical basis of this study were supported by Mr. Takashi Okano, Mie University, and the authors express their sincere appreciation for this foundational contribution.

Authors contributions: Research concept and design: T.K.; collection and/or assembly of data: S.K. and R.I.; data analysis and interpretation: S.K., R.I., and A.H.; writing the article: A.H.; critical revision of the article: T.K.; final approval of the article: T.K. and A.H. All authors have read and agreed to the published version of the manuscript.

Conflict of interest: The authors declare that they have no conflict of interest.

6. REFERENCES

Albrigo, L.G., Stelinski, L.L., Timmer, L.W., 2019. Citrus, 2nd ed. CABI, Oxford.

Bureau, S., Ruiz, D., Reich, M., Gouble, B., Bertrand, D., Audergon, J.M., *et al*., 2009. Application of ATR-FTIR for a rapid and simultaneous determination of sugars and organic acids in apricot fruit. Food Chem. 115, 1133-1140. https://doi.org/10.1016/j.foodchem.2008.12.100

Dilmaghani, M.R., Malakouti, M.J., Neilsen, G.H., Fallahi, E., 2005. Interactive effects of potassium and calcium on K/Ca ratio and its consequences on apple fruit quality in calcareous soils of Iran. J. Plant Nutrition, 27(7), 1149-1162. https://doi.org/10.1081/PLN-120038541

Kameoka, S., Isoda, S., Hashimoto, A., Ito, R., Miyamoto, S., Wada, G., *et al*., 2017. Wireless sensor network for growth environment measurement and multi-band optical sensing to diagnose tree vigor. Sensors 17, 966. https://doi.org/10.3390/s17050966

Kameoka, T., Hashimoto, A., 2015. Effective application of ICT in food and agricultural sector – Optical sensing is mainly described. IEICE Trans. Commun. E98-B, 1741-1748. http://doi.org/10.1587/transcom.E98.B.1741

Kameoka, T., Okuda, T., Hashimoto, A., Noro, A., Shiinoki, Y., Ito, K., 1998. A rapid FT-IR/ATR method for sugar content determination in food. Nippon Shokuhin Kagaku Kogaku Kaishi 45, 199-204. https://doi.org/10.3136/nskkk.45.199

Kanou, M., Kameoka, T., Suehara, K., Hashimoto, A., 2017. Mid-infrared spectroscopic analysis of saccharides in aqueous solutions with sodium chloride. Biosci. Biotechnol. Biochem. 81, 735-742. https://doi.org/10.1080/09168451.2016.1277943

Khalil, N.H., Hammoodi, J.K., 2020. Effect of nitrogen, potassium and calcium in strawberry fruit quality. Int. J. Agricult. Stat. Sci. 16 Supplement 1, 1967-1972. https://connectjournals.com/03899.2020.16.1967

Khojastehnazhand, M., Omid, M., Tabatabaeefar, A., 2009. Determination of orange volume and surface area using image processing technique. Int. Agrophys. 23, 237-242.

Lieten, P., 2006. Effect of K: Ca: Mg ratio on performance of 'Elsanta' strawberries grown on peat. In: Proc. Vth Int. Strawberry Symp.: Coolum Beach, Queensland, Australia, September 5-10, 2004 (No. 708). Int. Soc. Hort. Sci.

Marschner, H. (Ed.)., 2011. Marschner's mineral nutrition of higher plants. 3rd ed. Academic press, Amsterdam.

McLaren, T.I., Guppy, C.N., Tighe, M.K., 2012. A rapid and non-destructive plant nutrient analysis using portable X-ray fluorescence. Soil Sci. Soc. Am. J. 76, 1446-1453. https://doi.org/10.2136/sssaj2011.0355

Mendoza, F., Dejmek, P., Aguilera, J.M., 2006. Calibrated color measurements of agricultural foods using image analysis. Postharvest Biol. Technol. 41, 285-295. https://doi.org/10.1016/j.postharvbio.2006.04.004

Mizuno, T., Kondo, D., Kasai, H., Kuwabara, K., Yamashita, J., Murai, Y., *et al*., 2024. Concentrations and inter-element correlations of seven essential elements in wild plants of Japan. Ecol. Res. 39, 941-956. https://doi.org/10.1111/1440-1703.12533

Motonaga, Y., Kondou, H., Hashimoto, A., Kameoka, T., 2004. A method of making digital fruit color charts for cultivation management and quality control. Int. J. Food Agric. Environ. 2, 160-166.

Muramatsu, T., Suehara, K., Kameoka, T., Notaguchi, M., Hashimoto, A., 2020. Development of multiband optical sensing method for phenotyping of tomatoes in cultivation site. Food Res. 4 (S6), 132-137. https://doi.org/10.26656/fr.2017.4(S6).021

Najafi-Ghiri, M., Mirsoleimani, A., Boostani, H.R., Amin, H., 2022. Influence of wood vinegar and potassium application on soil properties and Ca/K ratio in citrus rootstocks. J. Soil Sci. Plant Nutrition 22(1), 334-344. https://doi.org/10.1007/s42729-021-00653-3

Nakai, I. (Ed.), 2016. X-ray Fluorescence Analysis Handbook (in Japanese). 2nd ed. Asakura Publishing, Tokyo.

Nakanishi, K., Hashimoto, A., Kanou, M., Pan, T., Kameoka, T., 2003. Mid-infrared spectroscopic measurement of ionic dissociative materials in metabolic pathway. Appl. Spectrosc. 57, 1510-1516. https://doi.org/10.1366/000370203322640152

Pathare, P.B., Opara, U.L., Al-Said, F.A.-J., 2013. Colour measurement and analysis in fresh and processed foods: A review. Food Bioprocess Technol. 6, 36-60. https://doi.org/10.1007/s11947-012-0867-9

Reidinger, S., Ramsey, M.H., Hartley, S.E., 2012. Rapid and accurate analyses of silicon and phosphorus in plants using a portable X-ray fluorescence spectrometer. New Phytol. 198, 699-706. https://doi.org/10.1111/j.1469-8137.2012.04179.x

Spiegel-Roy, P., Goldschmidt, E.E., 1996. The Biology of Citrus. Cambridge University Press, Cambridge. https://doi.org/10.1017/CBO9780511600548

Storey, R., Treeby, M.T., 2000. Seasonal changes in nutrient concentrations of navel orange fruit. Sci. Hortic. 84, 67-82. https://doi.org/10.1016/S0304-4238(99)00093-6

Taiz, L., Zeiger, E., 2017. Plant Physiology and Development, 6th ed. Sinauer Associates, Sunderland, MA.

Ting, S.V., 1969. Distribution of soluble components and quality factors in the edible portion of citrus fruits. J. Am. Soc. Hortic. Sci. 94, 515-519. https://doi.org/10.21273/JASHS.94.5.515

Ting, S.V., Rouseff, R.L., 1986. Citrus Fruits and Their Products: Analysis and Technology. Marcel Dekker, New York.

Yajima, Y., Wakabayashi, H., Suehara, K., Kameoka, T., Hashimoto, A., 2024. Simultaneous content determination of mono-, di- and fructo-oligo-saccharides in citrus fruit juices using an FTIR-PLS method based on selected absorption bands. Int. J. Food Sci. 9265590. https://doi.org/10.1155/2024/9265590

Yamamoto, K., Guo, W., Yoshioka, Y., Ninomiya, S., 2014. On plant detection of intact tomato fruits using image analysis and machine learning methods. Sensors 14, 12191-12206. https://doi.org/10.3390/s140712191

Zaresani, H., Sayyah, A.H.A., Zareiforoush, H., Khorramifar, A., Gancarz, M., Tabor, S., *et al*., 2024. Vis/NIR and FTIR spectroscopy supported by machine learning techniques to distinguish pure from impure Iranian rice varieties. Int. Agrophys. 38, 203-211. https://doi.org/10.31545/intagr/185392

Zimmermann, M.H., Milburn, J.A., 1975. Transport in Plants I: Phloem Transport, 1st ed. Springer, Berlin, Heidelberg. https://doi.org/10.1007/978-3-642-66161-7